

# SN Ia detection in the SNLS photometric analysis using Morphological Component Analysis

A. Möller,<sup>a,b,1</sup> V. Ruhlmann-Kleider,<sup>a</sup> F. Lanusse,<sup>c</sup> J. Neveu<sup>a</sup> and  
N. Palanque-Delabrouille<sup>a</sup>

<sup>a</sup>Irfu, SPP, CEA Saclay,  
F-91191 Gif sur Yvette cedex, France.

<sup>b</sup>Université Paris Diderot - Paris 7,  
75013 Paris, France.

<sup>c</sup>Laboratoire AIM, UMR CEA-CNRS-Paris 7, Irfu, SAp, CEA Saclay,  
F-91191 Gif sur Yvette cedex, France.

E-mail: [anais.moller@cea.fr](mailto:anais.moller@cea.fr), [vanina.ruhlmann-kleider@cea.fr](mailto:vanina.ruhlmann-kleider@cea.fr),  
[francois.lanusse@cea.fr](mailto:francois.lanusse@cea.fr), [jeremy.neveu@cea.fr](mailto:jeremy.neveu@cea.fr), [nathalie.palanque-delabrouille@cea.fr](mailto:nathalie.palanque-delabrouille@cea.fr)

**Abstract.** Detection of supernovae (SNe) and, more generally, of transient events in large surveys can provide numerous false detections. In the case of a deferred processing of survey images, this implies reconstructing complete light curves for all detections, requiring sizable processing time and resources. Optimizing the detection of transient events is thus an important issue for both present and future surveys. We present here the optimization done in the SuperNova Legacy Survey (SNLS) for the 5-year data differed photometric analysis. In this analysis, detections are derived from stacks of subtracted images with one stack per lunation. The 3-year analysis provided 300,000 detections dominated by signals of bright objects that were not perfectly subtracted. We developed a subtracted image stack treatment to reduce the number of non SN-like events using morphological component analysis. This technique exploits the morphological diversity of objects to be detected to extract the signal of interest. At the level of our subtraction stacks, SN-like events are rather circular objects while most spurious detections exhibit different shapes. A two-step procedure was necessary to have a proper evaluation of the noise in the subtracted image stacks and thus a reliable signal extraction. We also set up a new detection strategy to obtain coordinates with good resolution for the extracted signal. SNIa Monte-Carlo (MC) generated images were used to study detection efficiency and coordinate resolution. When tested on SNLS 3-year data this procedure decreases the number of detections by two, losing only 5% of SN-like events, all faint ones. MC results show that SNIa detection efficiency is equivalent to that of the original method for bright events, while the coordinate resolution is improved.

---

<sup>1</sup>Corresponding author.

---

## Contents

<b>1</b>	<b>Introduction</b>	<b>1</b>
<b>2</b>	<b>Morphological Component Analysis</b>	<b>2</b>
<b>3</b>	<b>Reducing artifacts in SNLS subtraction stacks</b>	<b>4</b>
3.1	First treatment	4
3.2	Second treatment	5
<b>4</b>	<b>New Detection strategy</b>	<b>6</b>
<b>5</b>	<b>Results</b>	<b>8</b>
5.1	SNLS data	8
5.2	Monte-Carlo efficiency and coordinate resolution	8
<b>6</b>	<b>Conclusions</b>	<b>9</b>

---

## 1 Introduction

Surveys of distant type Ia supernovae (SNe Ia) revealed at the end of the twentieth century the acceleration of the expansion of the Universe [1, 2]. Since then, other surveys such as SNLS and SDSS-II [3] have been set in place to obtain measurements of SNe Ia with higher precision. The first step for detecting SNe events is to make a sample of transient events to be later classified. Detection using only photometry with difference images, where a reference image is subtracted, provides a good approach. However, difference images are filled with various artifacts from instrumental defects and incomplete subtraction of permanent objects. Disentangling real transient events from artifacts becomes an important requirement especially for photometric only pipelines such as the one developed in the deferred analysis of SNLS [4].

SNLS is part of the Deep Synoptic Survey conducted on the Canada-France-Hawaii Telescope (CFHT). It was designed for detecting hundreds of SNe Ia in a redshift range between 0.2 and 1. Using the MegaCam imager [5], an array of 36 CCD with 340 million of pixels, four one square degree fields were targeted throughout 5 to 7 consecutive lunations per year using four different broadband filters  $g_M$ ,  $r_M$ ,  $i_M$  and  $z_M$  in the wavelength range from 400 to 1000  $nm$ . Images were preprocessed at CFHT to perform flat-fielding and to remove defects. These pre-processed images were submitted to different pipelines. The real-time one provides detections of SNIa candidates and includes the result of spectroscopic follow-up for further classification and redshift determination [6].

The deferred photometric pipeline is independent of this real time analysis. It is based only on photometry to detect and select SNe candidates assigning them host galaxy photometric redshifts from an external catalogue. The feasibility of detecting SNIa with this deferred analysis was proven for the 3-year SNLS data in [4]. In the era of large future surveys, spectroscopic resources will be limited for candidate follow-up and classification, which makes photometric pipelines interesting to study, e.g. [7].

The SNLS photometric pipeline is described in more detail in [4]. In the following we will summarize the main features relevant to our study. Detection of transient events is done

only in the  $i_M$  filter because distant SNe in SNLS have their maximum flux in this band. Reference images are constructed for each field from a set of best quality images which are coadded. Each image of the survey has the reference image subtracted. The subtraction is done using determination of the sky background and a convolution kernel which allows the subtraction to be adapted to different observing conditions. In order to increase the signal-to-noise ratio, subtracted images for each lunation are stacked. Lunation detection catalogues are constructed from these subtracted image stacks keeping only events which have a S/N ratio of  $2.5 \sigma$  w.r.t. the sky background. The final detection catalogue is obtained by merging all lunation catalogues. All detection catalogues are constructed using SExtractor [8].

For the SNLS 3-year (SNLS3) analysis [4], the detection resulted in 300,000 transient candidates for which four-filter light curves were reconstructed. However, detections were dominated by spurious objects due to bad subtraction. Spurious detections came mostly from imperfectly subtracted objects such as bright stars, resampling defects and masks (see e.g. Figures 1, 2). Therefore, in order to reduce the number of detections, it is necessary to disentangle true signal from artifacts in subtracted image stacks.

In this paper we present a new approach for improving transient event detection based on morphological component analysis [9] for difference image stacks in the SNLS survey. We exploit the different morphologies of objects in the stacks to separate transient objects from artifacts. Other methods to achieve such a goal exist, such as the one recently introduced by [10] based on machine learning and principal component analysis using SDSS images. We also describe how we extract signal coordinates with good resolution from the subtracted image stacks after our new processing.

The outline of the paper is as follows. Morphological component analysis is introduced in Section 2. The method proposed to clean subtracted image stacks in order to severe spurious detections is presented in Section 3. Section 4 describes the new detection strategy based on the cleaned stacks. Results on SNLS3 data and MC efficiency and coordinate resolution studies are presented in Section 5.

## 2 Morphological Component Analysis

The Morphological Component Analysis (MCA) framework assumes that an observed image can be described as the sum of several components, each exhibiting a distinct morphology. The aim of MCA is to leverage these characteristic morphologies to disentangle the different components of an image. More formally, given an image  $X$ , assumed to be the sum of  $K$  morphologically different components  $x_k$ ,

$$X = \sum_{k=1}^K x_k, \quad (2.1)$$

morphological component analysis can be used to recover each individual contribution  $x_k$ . In the context of SN detection in image stacks, this approach can be used to disentangle transient objects from artifacts as they exhibit different morphologies.

To actually perform this separation, MCA relies on the theory of sparse representation of signals. Any signal can be represented in a number of different domains (e.g. time domain, Fourier domain, wavelet domain) but the coefficients of this signal will exhibit different properties depending on the domain. One property of particular interest is the so called sparsity of the coefficients, i.e. the property that only a small number of coefficients are non zero.

As a general rule, the coefficients of the signal will be sparse when the basis functions of the domain (so called *atoms*) are very similar to the signal itself.

In fact, this sparsity property is extremely desirable as it can be used as a very powerful prior in the regularization of a wide range of inverse problems. Some applications to astronomy and astrophysics include denoising [11], deconvolution [12], blind source separation for CMB analysis [13], weak gravitational lensing [14].

More formally, let us note  $\alpha$  the coefficients of a signal  $x$  in a *dictionary*  $\Phi$  (a dictionary being the set of atoms  $\phi_i$  of a given domain):

$$x = \Phi\alpha = \sum_i \phi_i \alpha_i, \quad (2.2)$$

If  $x$  is sparse in dictionary  $\Phi$  then only a small number of coefficients in  $\alpha$  are non zero. Given image  $X$  defined in (2.1) as the sum of  $K$  different morphological components, let us introduce  $K$  different dictionaries  $\Phi_k$ , each adapted only to the particular morphology of component  $x_k$  i.e. such that the  $\alpha_k$  coefficients,  $\{\alpha_{ki}\}$ , of  $x_k$  in  $\Phi_k$  are sparse but not the coefficients of  $x_l$  for  $l \neq k$ . Then performing the separation of the different morphological components can be achieved by finding an optimal set of coefficients  $\alpha_k$  maximizing the sparsity of the decomposition of each component in the corresponding dictionary.

The Morphological Component Analysis (MCA) algorithm has been proposed by [15] as a practical way to perform this decomposition as the solution of an  $\ell_1$  minimisation problem, where  $\ell_1$  denotes the  $\ell_1$ -norm. Observed images,  $Y$ , are assumed to be a combination of signals,  $X$ , plus some noise,  $N$ . The decomposition algorithm solves iteratively the following optimization problem:

$$\min_{\mathbf{x}_1, \dots, \mathbf{x}_K} \sum_{k=1}^K \|\Phi^* \mathbf{x}_k\|_1 \quad \text{such that} \quad \|Y - \sum_{k=1}^K \mathbf{x}_k\|_2 \leq \sigma, \quad (2.3)$$

where  $\Phi^* \mathbf{x}_k = \alpha_k$  and  $\sigma$  is the standard deviation of the noise contaminating the data, assumed to be stationary and Gaussian distributed. The  $\ell_1$ -norm promotes the sparsity of the decomposition of each component [16]. At convergence, each morphological component is obtained as  $x_k = \Phi_k \alpha_k$ . This component reconstruction can be restricted to a sub-sample of  $\{\alpha_{ki}\}$ , for example to some size scales in a given dictionary.

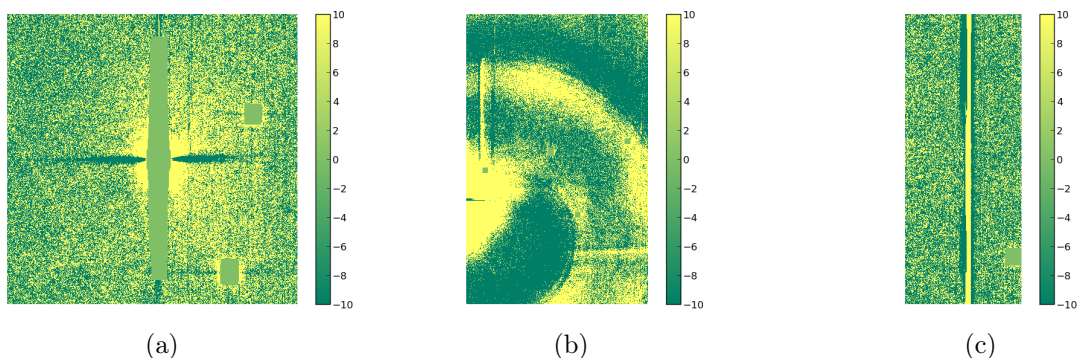


**Figure 1:** Different defects on the subtracted image stacks that yield spurious detections on large scale: (a) shows a saturated star with some areas masked by subtraction, (b) a saturated star plus the camera mounting shadow and (c) defects from sampling and dead pixel lines.

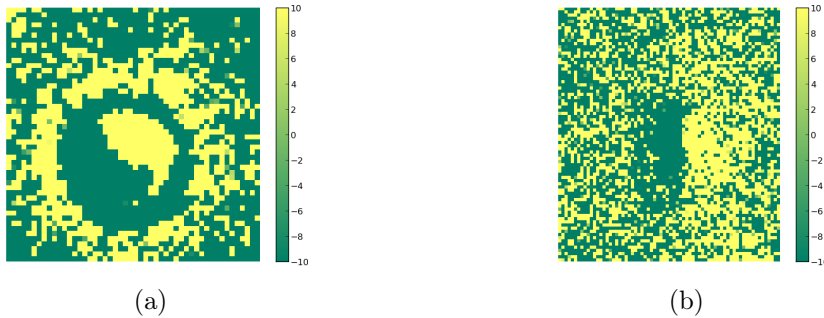


**Figure 2:** Defects on the subtracted image stacks that yield spurious detections on small scale: (a) and (b) dipoles from imperfect galaxy subtraction. These are adjacent positive and negative areas on the stacks.

### 3 Reducing artifacts in SNLS subtraction stacks

Morphological component analysis allows to disentangle artifacts from other signals and can be adapted to treat subtracted image stacks in SNLS. In our subtracted image stacks, artifacts, which are the most common cause of spurious detections, have particular shapes and sizes, see Figure 1 for large scale defects and Figure 2 for small scale ones. Meanwhile SNe are small scale circular type shaped objects.

We present hereby a two-step treatment based on MCA to simultaneously reduce artifacts and to extract interesting SN-like signals.

#### 3.1 First treatment

The MCA algorithm in [15] was adapted to treat our subtracted image stacks. The chosen dictionaries for the decomposition were: starlets, bi-orthogonal wavelets, curvelets and ridgelets [17]. The number of decomposition scales, corresponding to the number of atoms in equation 2.2, was chosen to be 5 in dictionaries which represent mostly artifacts (curvelets, ridgelets), and 3 for the starlets which efficiently decompose circular-like signals as can be seen in Figure 3. Both positive and negative signals were decomposed since some SNe may have part of their flux included in the references, in which case subtraction yields a negative signal.

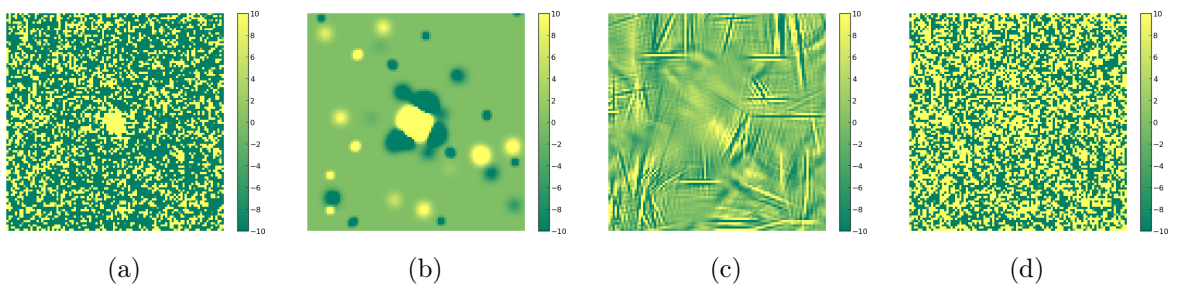


**Figure 3:** MCA Decomposition of a SNIa event. (a) shows the original subtracted image stack, (b) the starlet component, (c) the curvelet component and (d) the residuals left after the decomposition.

Adapting the algorithm parameters required a thorough study on real data and many trials. We used as a test-sample the SNLS3 data in the D4 field. The choice of parameters

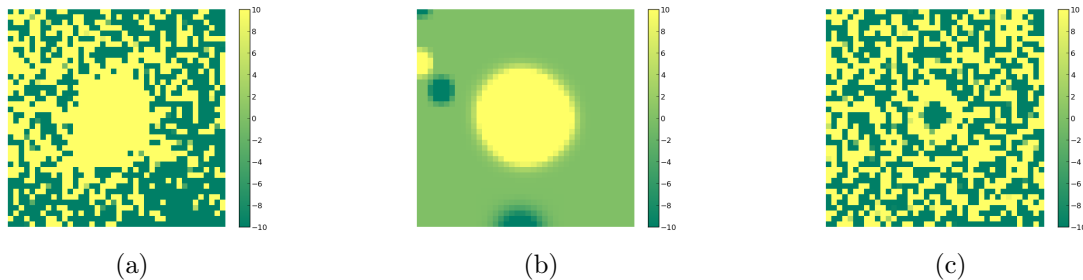


**Figure 4:** MCA Decomposition of a SNIa event where some part of the signal leaks to residuals. (a) shows the original subtracted image stack, (b) the starlet component and (c) the residuals after decomposition containing part of the signal.

(e.g. the number of iterations, scales chosen for each dictionary, transformation thresholds) resulted from a trade-off between reducing the total number of detections and keeping most of the SN-like objects identified in [4]. A compromise between number of iterations and computation time was achieved with 30 iterations for the decomposition. The transforms used in the algorithm, especially that of the curvelet dictionary, do not scale well with the image size and too much CPU time and memory would be required for a SNLS survey image of 2176 by 4912 pixels. Therefore, tiling of the images was done both to reduce time and memory resources and to allow parallel processing. For reference, one SNLS image divided in 8 tiles requires on average 6 days of HS06 CPU time and 500 Mb of virtual memory to be treated.

The algorithm assumes a stationary and Gaussian noise in the input images which is not the case for our subtracted image stacks, that are built from the coaddition of subtracted images spanning several weeks of observations. Thus, the signal we aimed at recovering was not properly decomposed and was partially in the residuals, e.g. Figure 4. To tackle this, a second treatment was developed which uses as input the starlet component and the residuals of our first treatment decomposition (e.g. components (b) and (d) of Figure 3).

### 3.2 Second treatment

A utility based on the algorithm in [17] was developed. It handles non-stationary noise and exploits further morphological decomposition. Non-stationary noise requires varying the threshold in the decomposition depending on the position of the analyzed pixel. Such a feature can be easily implemented in the wavelet dictionary since it can easily handle actual noise maps. The latter were computed from the first treatment output images using a median absolute deviation estimator. This computation used a sliding window with a fixed size larger than what is expected for a SN-like signal. Since some of the SNe may have part of their flux included in the references, both positive and negative signals were treated.

We used the starlet dictionary in order to filter out low coefficient transformations while reinforcing sparsity. All signals present in the output can be considered as morphologically compatible with circular-like objects. An example can be seen in Figure 5.

This utility does not require tiling images since only the wavelet dictionary is used. One SNLS image takes on average 3 hours of HS06 CPU time and 100 Mb of virtual memory to be treated.

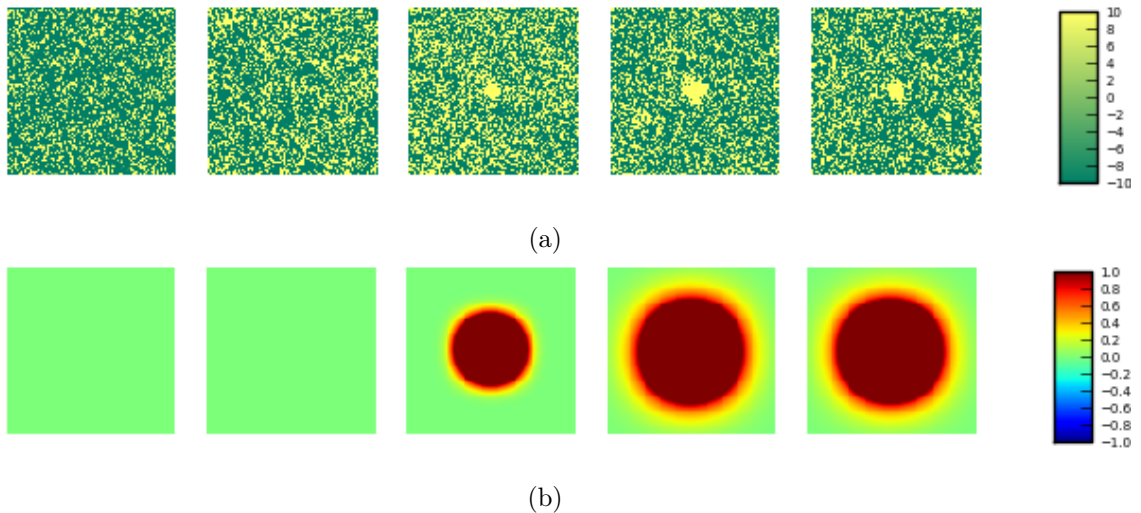


**Figure 5:** A SNIa event shown in different lunations around maximum light in the original subtracted image stack (a) and after the second step of the cleaning procedure (b).

#### 4 New Detection strategy

A detection strategy includes both extracting events from an image and reconstructing their coordinates. Event extraction depends on the image and its characteristics, e.g. its local noise information. The TERAPIX tool SExtractor [8] was used for the whole detection strategy both in the original procedure and the new procedure adjusting its parameters accordingly.

In [4] the detection strategy consisted in constructing lunation catalogues with SExtractor with deblending, requiring for each detection at least 4 pixels with signal of more than  $2.5\sigma$  w.r.t. sky background. A final detection catalogue was obtained by merging all lunation catalogues obtained in three years and converting the result into an image where each detection was replaced by a Gaussian of height and width of 1. This image was processed with SExtractor selecting only pixels with a content above a value of 0.01 and deblending objects. In this way, any object detected on several lunations at the same position (within a pixel) gave only one detection, with a position averaged over all lunation stacks. This is described on the top part of Figure 6.

Our two-step treatment outputs image stacks which do not have the same properties as the original subtracted image stacks. The noise has been removed and sources are reconstructed using inverse transformations. As transformed images they have less objects but coordinates cannot be extracted accurately from them. We thus propose a new detection strategy (see Figure 6 bottom) which also addresses the degradation of coordinate resolution when using several years of data.

Lunation catalogs are constructed from our cleaned subtraction stacks using SExtractor, requiring at least 200 pixels with a signal value above one to confirm an object. Deblending is imposed in order to separate adjacent objects. To each object in a lunation we assign the coordinates of the closest detection in the same lunation catalogue of the original procedure. In this way we maintain the reduced number of candidates while having precise coordinates.

In the original procedure coordinates were averaged over all lunations which degrades signal coordinate resolution due to close-by spurious detections, as can be seen in Figure 7. When adding data from other seasons, this degradation becomes even more important.

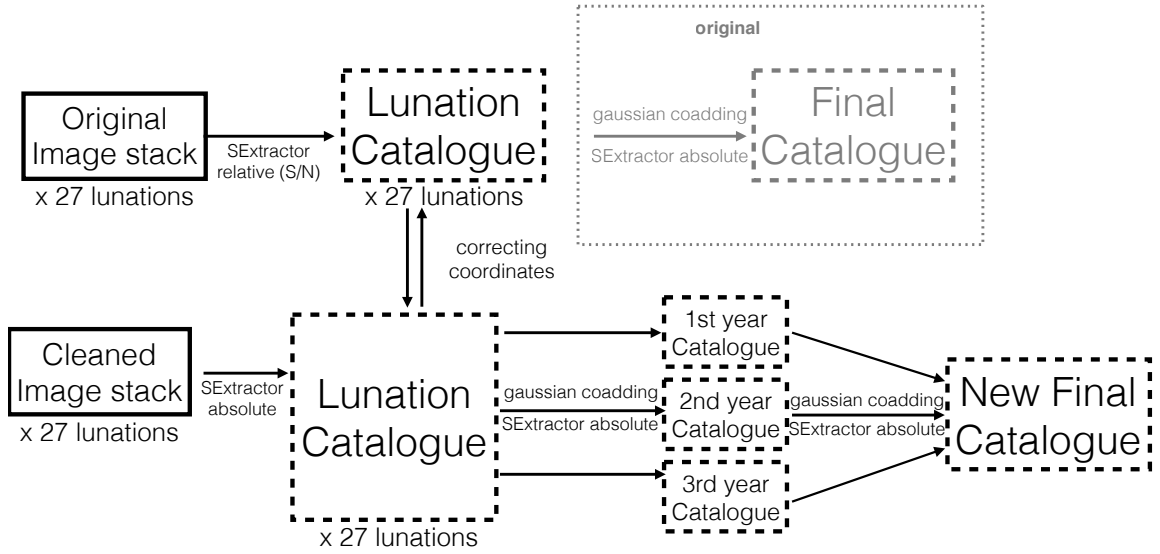


**Figure 6:** New detection strategy schema. Doted lines represent catalogue ASCII files while continuous lines images.

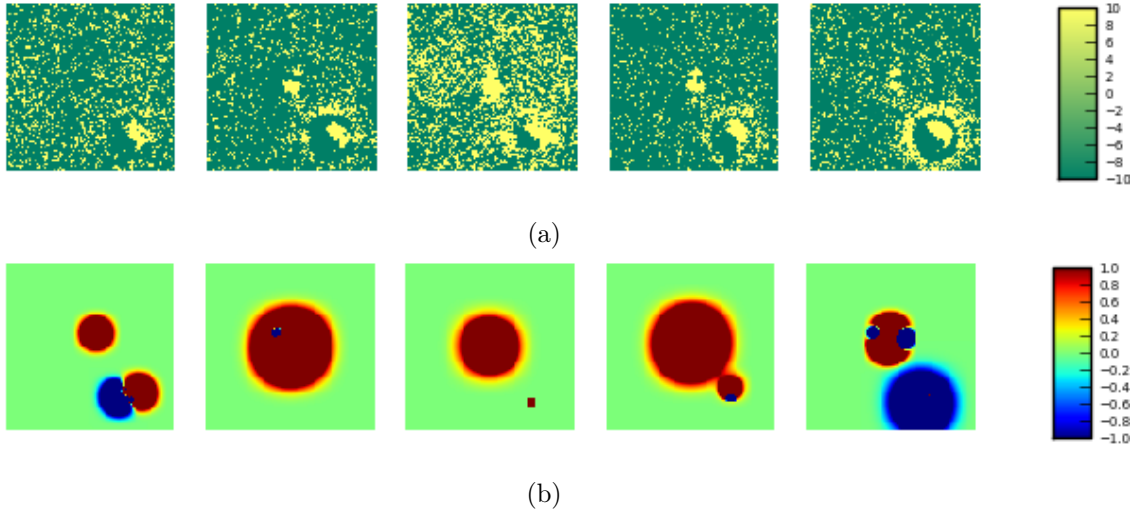


**Figure 7:** A SNIa event (center of the image) with galaxy residuals shown in different lunations around maximum light in the original subtracted image stacks (a) and after cleaning (b). In the original stacks, galaxy residuals are present in all lunations. The cleaning removes them in some cases.

Real SN-like events can be present in at most three adjacent lunation catalogs but not over several seasons. Hence, to address this in the new procedure we first build a catalogue for each season as we did for the final catalogue in the original procedure. Then, we build the new final catalogue from the season catalogues in the same way.

In this way, coordinate averaging is done first for a season were a transient object can

Stack	Old procedure		New procedure	
	coordinate resolution	magnitude bias	coordinate resolution	magnitude bias
1-year	$0.374 \pm 0.002$	$0.0093 \pm 0.0001$	$0.368 \pm 0.002$	$0.0090 \pm 0.0001$
3-year	$0.392 \pm 0.002$	$0.0104 \pm 0.0001$	$0.381 \pm 0.002$	$0.0096 \pm 0.0001$
5-year	$0.410 \pm 0.002$	$0.0118 \pm 0.0001$	$0.394 \pm 0.002$	$0.0100 \pm 0.0001$

**Table 1:** Coordinate resolutions (pixels) and corresponding magnitude bias of SNIa detection original and new procedures: for year 3 MC data (1-year stack), adding two additional years of data (3-year stack) and adding 4 additional years of data (5-year stack). Uncertainties shown here are from the statistics of generated SNIa.

be present and then detections are added from other years. It is equivalent to assigning a weight for a given detection taking into account that a SN will be detected only during one season.

## 5 Results

### 5.1 SNLS data

The SNLS3 D4 test sample contained 90.971 detections from which 362 events were extracted as SN-like objects as described in [4]. After our processing, the number of detections is reduced to 40.575. This represent more than a factor 2 reduction on the number of candidates to be further processed. Loss of SN-like candidates is less than 5% and all lost events are faint (observed magnitude at peak in  $i_M > 24.2$ ) and so not suitable for further cosmological analysis.

### 5.2 Monte-Carlo efficiency and coordinate resolution

The performance of our treatment was studied using MC artificial images in the  $i_M$  filter generated in the D1 field [18]. The MC images were constructed by adding simulated supernovae to real images, on positions chosen from an external catalogue of host galaxies identified from deep image stacks of the CFHT-LS Deep Fields [19]. The redshift was restricted to the range between 0.2 and 1.2. Images were processed by our optimized pipeline and compared to results from the original procedure described in [4].

Detection efficiency was defined as the fraction of recovered simulated supernovae at the end of each processing. For both the original and the new procedure we computed the detection efficiency for one year of simulated SNe Ia as a function of the generated SN peak magnitude as can be seen in Figure 8. The efficiency is nearly magnitude independent up to  $m_{0i} = 23.5$  and then steeply declines at faint magnitudes. When compared to the old procedure, the new procedure corresponds to a loss of 0.5% in the plateau efficiency and a 0.2 downward shift of the magnitude corresponding to 0.50 efficiency.

The SNIa coordinate resolution was studied for both procedures as can be seen in Table 1. The resolution was given by the RMS of the distance between the coordinate at generation and at detection. The coordinate resolution for one year simulated SNe Ia in our new pipeline was found to be  $0.368 \pm 0.002$  pixels to be compared to  $0.374 \pm 0.002$  pixels in the original pipeline. We also studied the effect of adding other years of survey data (without simulated SN signal), constructing catalogues with two or 4 additional years. A degradation of coordinate resolution is seen but the new procedure handles better many years of data than the original one.

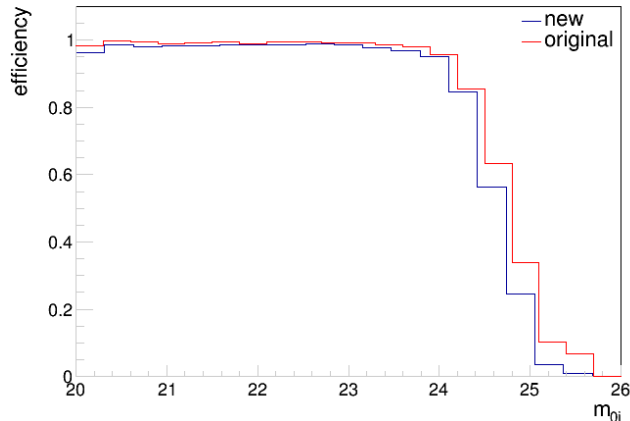


**Figure 8:** Efficiency of detection as a function of the generated peak magnitude in  $i_M$ . The new procedure (blue line) is compared to the original one (red line).

Position measurement inaccuracy leads to underestimated fluxes. Using appendix B of [20] we computed an indicative magnitude bias corresponding to our coordinate resolution. Results can be seen in Table 1. Thanks to the improved coordinate resolution, the new procedure applied on 5-year stacks has similar performance to the old procedure applied on 3-year stacks. The latter was found accurate enough for photometric typing as shown in [4]. The application of the new procedure to the whole set of SNLS data will be the subject of a future work.

## 6 Conclusions

In this paper we presented a new procedure for detecting supernovae in the SNLS photometric analysis. We developed a two-step procedure for cleaning subtracted image stacks, reducing artifacts and extracting SN-like signals using morphological component analysis. A new detection strategy, adapted to the cleaned image stacks was also presented.

The performance of the new procedure was evaluated using MC artificial images. Detection efficiency of SNIa in the old and the new procedure is almost unchanged for bright events, however there is a small reduction for events at higher magnitudes. When cross-checked with a test sample of SNLS3 data, only a few percent of SN-like faint events were lost while the number of detections was reduced by more than a factor two. Coordinate resolution of SNIa events was equivalent for one year of MC for both procedures. Furthermore, since SNLS is a five-year survey coordinate resolution was also studied adding other years of data. The new procedure yields slightly better SNIa coordinate resolution with respect to the original procedure when adding 4 additional years of data, simulating a five-year stack. Therefore, for a five-year photometric analysis this new procedure yields a slightly smaller magnitude bias for SNe Ia when compared to the original procedure.

Morphological component analysis has proven to be a useful approach for cleaning subtracted image stacks such as the ones in the SNLS deferred processing. Our experience shows that the precise nature of the input images is a key point when choosing and adapting this

type of algorithms. Once the algorithms are chosen, tuning their parameters require extensive study.

Finally, we note that eliminating artifacts at the level of subtracted images, instead of stacks, can be another way to improve detection efficiency. However, this should be applied at the beginning of the survey. For implementing such methods, a thorough analysis must be done of the trade-off between the gain on signal extraction and removal of artifacts with respect to the high computational and time costs of processing using dictionary decomposition.

## Acknowledgments

We thank J.-L. Starck for useful advice on MCA and comments on this paper.

This work was done based on observations obtained with MegaPrime/MegaCam, a joint project of CFHT and CEA/IRFU, at the Canada-France-Hawaii Telescope (CFHT) which is operated by the National Research Council (NRC) of Canada, the Institut National des Science de l'Univers of the Centre National de la Recherche Scientifique (CNRS) of France, and the University of Hawaii. This work is based in part on data products produced at Terapix available at the Canadian Astronomy Data Centre as part of the Canada-France-Hawaii Telescope Legacy Survey, a collaborative project of NRC and CNRS.

## References

- [1] **Supernova Cosmology Project** Collaboration, S. Perlmutter et al., *Measurements of Omega and Lambda from 42 high redshift supernovae*, *Astrophys.J.* **517** (1999) 565–586, [[astro-ph/9812133](#)].
- [2] **Supernova Search Team** Collaboration, A. G. Riess et al., *Observational evidence from supernovae for an accelerating universe and a cosmological constant*, *Astron.J.* **116** (1998) 1009–1038, [[astro-ph/9805201](#)].
- [3] **SDSS Collaboration** Collaboration, M. Betoule et al., *Improved cosmological constraints from a joint analysis of the SDSS-II and SNLS supernova samples*, *Astron.Astrophys.* **568** (2014) A22, [[arXiv:1401.4064](#)].
- [4] G. Bazin, V. Ruhlmann-Kleider, N. Palanque-Delabrouille, J. Rich, E. Aubourg, et al., *Photometric selection of Type Ia supernovae in the Supernova Legacy Survey*, *Astron.Astrophys.* **534** (2011) A43, [[arXiv:1109.0948](#)].
- [5] O. Boulade, X. Charlot, P. Abbon, S. Aune, P. Borgeaud, P.-H. Carton, M. Carty, J. Da Costa, H. Deschamps, D. Desforge, D. Eppelle, P. Gallais, L. Gosset, R. Granelli, M. Gros, J. de Kat, D. Loiseau, J. . Ritou, J. Y. Rousse, P. Starzynski, N. Vignal, and L. G. Vigroux, *Megacam: the new canada-france-hawaii telescope wide-field imaging camera*, vol. 4841, pp. 72–81, 2003.
- [6] **SNLS Collaboration** Collaboration, P. Astier et al., *The Supernova legacy survey: Measurement of omega(m), omega(lambda) and W from the first year data set*, *Astron.Astrophys.* **447** (2006) 31–48, [[astro-ph/0510447](#)].
- [7] H. Campbell, C. B. D’Andrea, R. C. Nichol, M. Sako, M. Smith, et al., *Cosmology with Photometrically-Classified Type Ia Supernovae from the SDSS-II Supernova Survey*, *Astrophys.J.* **763** (2013) 88, [[arXiv:1211.4480](#)].
- [8] E. Bertin and S. Arnouts, *SExtractor: Software for source extraction*, *Astron.Astrophys.Suppl.Ser.* **117** (1996) 393–404.
- [9] J.-L. Starck, M. Elad, and D. Donoho, *Redundant multiscale transforms and their application for morphological component separation*, *Adv.Imaging Electron Phys.* (2004).

- [10] L. d. Buisson, N. Sivanandam, B. Bassett, and M. Smith, *Machine Learning Classification of SDSS Transient Survey Images*, [arXiv:1407.4118](#).
- [11] S. Beckouche, J.-L. Starck, and J. Fadili, *Astronomical Image Denoising Using Dictionary Learning*, *Astron.Astrophys.* **556** (2013) A132, [[arXiv:1304.3573](#)].
- [12] J. Schmitt, J.-L. Starck, J.-M. Casandjian, J. Fadili, and I. Grenier, *Multichannel Poisson denoising and deconvolution on the sphere : Application to the Fermi Gamma Ray Space Telescope*, *Astron.Astrophys.* **546** (2012) A114, [[arXiv:1206.2787](#)].
- [13] J. Bobin, J.-L. Starck, F. Sureau, and S. Basak, *Sparse component separation for accurate CMB map estimation*, *Astron.Astrophys.* **550** (2013) 73, [[arXiv:1206.1773](#)].
- [14] A. Leonard, F. Lanusse, and J.-L. Starck, *GLIMPSE: Accurate 3D weak lensing reconstructions using sparsity*, *Mon.Not.Roy.Astron.Soc.* **440** (2014) 1281, [[arXiv:1308.1353](#)].
- [15] J.-L. Starck, M. Elad, and D. Donoho, *Image decomposition via the combination of sparse representations and a variational approach*, *IEEE Trans.Image Process.* **14** (2005) 1570–1582.
- [16] J.-L. Starck, F. Murtagh, and J. Fadili, *Sparse Image and Signal Processing: Wavelets, Curvelets, Morphological Diversity*. Cambridge University Press, New York, NY, USA, 2010.
- [17] J. Starck, F. Murtagh, and A. Bijaoui, *Image Processing and Data Analysis: The Multiscale Approach*. Cambridge Univ. Press, 1998.
- [18] P. Ripoche, *PhD thesis*. Université de Marseille, 2007.
- [19] O. Ilbert, S. Arnouts, H. McCracken, M. Bolzonella, E. Bertin, et al., *Accurate photometric redshifts for the cfht legacy survey calibrated using the vimos vlt deep survey*, *Astron.Astrophys.* **457** (2006) 841–856, [[astro-ph/0603217](#)].
- [20] **SNLS Collaboration** Collaboration, J. Guy et al., *The Supernova Legacy Survey 3-year sample: Type Ia Supernovae photometric distances and cosmological constraints*, *Astron.Astrophys.* **523** (2010) A7, [[arXiv:1010.4743](#)].